PROCEEDINGS OF SCIENCE

# Probing the Origin of North Polar Spur by Broadband Radio Observation: New Insight into Future X-ray and Gamma-ray Observations

**Ryoji Iwashita,**[a,*] **Jun Kataoka**[a] **and Yoshiaki Sofue**[b]

[a] *Faculty of Science and Engineering, Waseda University,*
*3-4-1 Okubo, shinjyuku, Tokyo 169-8555, Japan*
[b] *Institute of Astronomy, The University of Tokyo,*
*2-21-2 Osawa, Mitaka-shi, Tokyo 181-0015, Japan*
*E-mail:* u.rock.r21@fuji.waseda.jp, kataoka.jun@waseda.jp, sofue@ioa.s.u-tokyo.ac.jp

The North Polar Spur (NPS) is a large-scale structure that is clearly visible in both radio and X-ray all-sky maps. 22 MHz to 70 GHz broadband radio observations have been used to systematically analyze the thermal/nonthermal radiations associated with the NPS. We show that the radio emissions of NPS comprises (1) synchrotron radiation, (2) free-free radiation, and (3) dust emission; however synchrotron radiation dominate over other emissions, especially at high galactic-latitudes. In addition, the synchrotron spectra exhibit a power-law behavior $N(\gamma) \propto \gamma^{-s}$ ($s \simeq 2.2 - 3.0$), which is moderated by a turnover at $\nu \simeq 1$ GHz, above which the spectral index $s$ decreases by one. Assuming that the turnover is due to the electrons cooled by synchrotron emission before escaping (or advecting) from the emission region, the strength of the magnetic field can be estimated to be $B \simeq 8\mu$G if the NPS radiates from the Galactic Center (GC). However, an unreasonably strong $B \simeq 114\mu G$ is required if the NPS is near a local supernova remnant (SNR). We estimated the non-thermal energy stored in the NPS to be $E_{\rm n/th} \sim 4.3 \times 10^{55}$ erg in the GC scenario, whereas $E_{\rm n/th} \sim 4.1 \times 10^{52}$ erg is difficult to explain with a single local SNR. We also estimated the gamma-ray radiation associated with the NPS, through inverse Comptonization (IC) of the cosmic microwave background (CMB), which peaks at 100-1000 keV with a flux of $\nu F_\nu \sim 10^{-9}$ erg cm$^{-2}$s$^{-1}$sr$^{-1}$ in the GC scenario, which may be a good candidate for detection by future X-ray/gamma-ray observatories.

**** 7th Heidelberg International Symposium on High-Energy Gamma-Ray Astronomy ****
**** 4-8 July 2022 ****
**** Universitat de Barcelona, Barcelona, Spain ****

[*] Speaker

© Copyright owned by the author(s) under the terms of the Creative Commons Attribution-NonCommercial-NoDerivatives 4.0 International License (CC BY-NC-ND 4.0).



PoS(Gamma2022)145

## 1. Introduction

The North Polar Spur (NPS)/Loop I is a large-scale structure that is clearly visible in both radio and X-ray all-sky maps. Loop I is a large northward radiation structure that spans $\sim 120^\circ$ in the sky, and the brightest part of these regions is called the NPS. Although half a century has passed since its discovery, two competing ideas have been actively debated to postulate its origin. One of there is a supernova remnant (SNR) near the solar system (100 $\sim$ 200pc) [1]. According to this scenario, the NPS is attributed to supernova activity, and several authors have concluded that it is a collection of gas and dust expanded by a supernova explosion and stellar wind. An alternative scenario has been proposed, in which the NPS could be rerated to the activity in AGN and/or starburst outflows from the Galactic Center (GC) over 10 Myr ago [2]. The recent discovery of a series of structures from the GC, such as the Fermi Bubbles, popularized this theory. It has been suggested that the NPS is located along the edges of these galactic structures, indicating that bubble structure and NPS have the same origin from the galactic explosions.

Suzaku X-ray observations of the NPS are well reproduced by assuming three components of thermal radiation: (1) A local Bubble and solar wind charge exchange, (2) thermal emission and Galactic Halo (GH), and (3) a cosmic X-ray background [3, 4]. Although NPS analyses have been performed at single or a few wavelengths in the radio band, broadband analysis over multiple wavelengths has not yet been performed. In this study, we aim to clarify the NPS emission mechanism and obtain a closer insight into its origin by combining NPS radio data over multiple wavelength and analyzing the corresponding spectra.

## 2. Radio Data

We used 6 all-sky maps from 22 MHz to 2.3 GHz taken on the ground, data at 23 GHz was obtained with the WMAP satellite, and data at 30GHz $\cdot$ 44GHz $\cdot$ 70GHz obtained with the Planck satellite. The 23 GHz of WMAP was separated into synchrotron and free-free radiation using the Maximum Entropy Method (MEM) analysis [5]. The all-sky maps were converted to a Mercator diagram, then the resolution of all maps was converted to $(l \times b) = (1^\circ \times 1^\circ)$ per pixel ($180 \times 360$ pixels). The mean of the obtained data within a pixel was taken as the measured value, and the standard deviation was the error at that pixel. Moreover, the Cosmic Microwave Background (CMB; $T_{CMB} = 2.7$ K) was uniformly subtracted from the data. Because some of the brightness temperature data of Planck contained negative values that were consistent with zero within uncertainties, all negative values were set to zero. When the lower limit of the error bar was negative, the upper limit was considered for the analysis.

## 3. Spectral Analysis

Spectra were produced for regions varying in galactic-longitude by $20^\circ$, and the galactic-longitude was fixed at $30^\circ$ where the NPS radiation is the brightest (Figure 1). Then, the spectral region is taken to be $1^\circ$ in both the galactic-longitude and galactic-latitude regions. As a result, NPS emission decreases following a $\beta \simeq 2.6 - 3.0$ ($T_b \propto \nu^{-\beta}$) power-law up to a few GHz, regardless of the galactic-latitude. Moreover, cut-offs were observed around 1 GHz, especially at high galactic-latitudes. The 23 GHz data showed that the free-free emission dominated at low galactic-latitudes,



PoS(Gamma2022)145

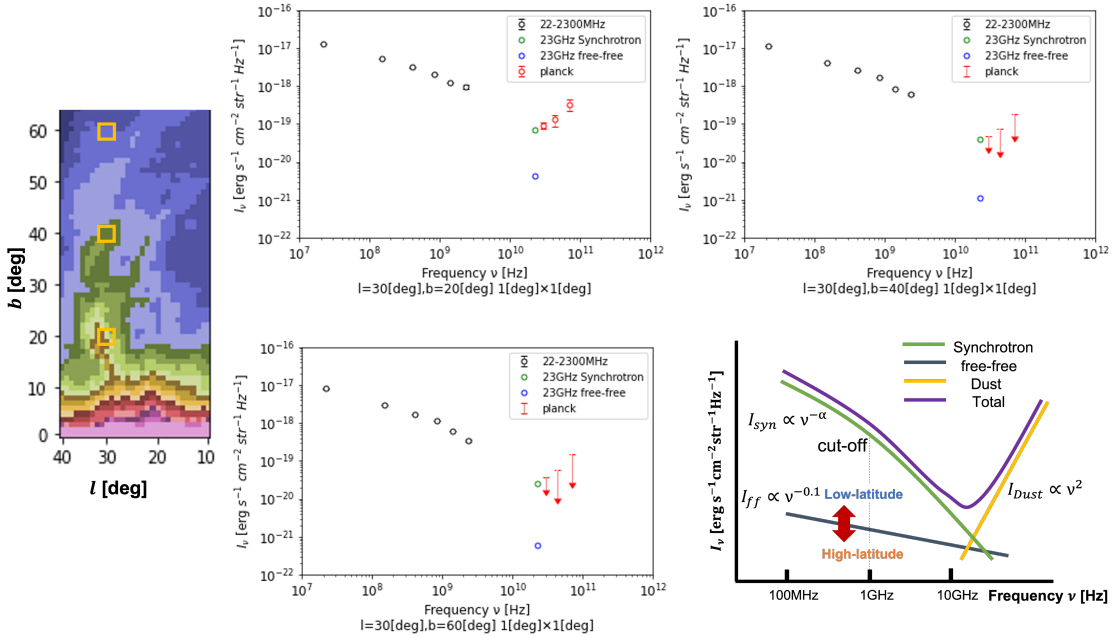


**Figure 1:** Spectra of the NPS in the radio band. The figure shows typical spectra for every 20° of galactic-latitude. Left: Haslam's 408 MHz sky map with spectral regions. Bottom-Right: Characteristics of the NPS radio spectrum.

and synchrotron radiation dominated at high galactic-latitudes. Free-free emission exhibited a flat power-law $\alpha \simeq -0.1$ ($I_\nu \propto \nu^\alpha$) in the optically thin region, whereas synchrotron radiation exhibited a significantly steeper power-law behavior with $\alpha > -1.0$. Therefore, synchrotron radiation clearly dominates at high galactic-latitudes and up to a few GHz.

We consider the 30-70 GHz Planck data where the radiation was consistent with the thermal radiation from dust with $\alpha \simeq 2.0$ power-law. In the optically thin limit, the Spectral Energy Distribution (SED) of the emission from a uniform population of grains is well described empirically by a modified blackbody $I_\nu = \tau_\nu B_\nu(T)$, where $\tau_\nu$ is the frequency-dependent dust optical depth, and $B_\nu$ is the Planck function for dust at temperature. The characteristics of the NPS radio spectrum obtained from there results are shown in the bottom-right panel of Figure 1.

## 4. Discussion

### 4.1 Spectral turnover

The origin of spectral turnover identified in the NPS spectra is discussed in terms of synchrotron cooling. When the transport equation for electrons near the shock is expressed in the Leaky-Box model, the solution can be expressed approximately as follows [6]

$$N_e(\gamma > \gamma_{\rm min}) = N_0 \gamma^{-s} \left(1 + \frac{\gamma}{\gamma_{\rm brk}}\right)^{-1} \times \exp\left(\frac{\gamma}{\gamma_{\rm max}}\right). \quad (1)$$

Here, $s$, $N_0$, and $\gamma_{\rm min}$ (or $\gamma_{\rm max}$) denote the injection index, normalization constant, and minimum (or maximum) electron energy. Then, $\gamma_{\rm brk}$ corresponds to the energy at which the electron cooling



PoS(Gamma2022)145

time and advection time are balanced ($t_{\rm cool} \simeq t_{\rm adv}$), resulting in an electron distribution with a turnover whose power-law index $s$ decreases by one. If the spectral turnover $\gamma_{\rm brk}$ originates from synchrotron cooling, the magnetic field $B$ can be estimated by balancing the advection and cooling time scales of electrons.

In a non-relativistic strong shock wave, the compression ratio is $v_2/v_1 = 1/4$, where $v_1$ and $v_2$ are the upstream and downstream velocities in the rest frame of the shock, respectively. The advection time of electrons can be expressed as $t_{\rm adv} \simeq R/v_2 = 4R/v_1$ [s], where $R$ denotes the thickness of the radiating area. The electron cooling time owing to synchrotron emission is $t_{\rm cool} \simeq E/(dE/dt) = 3\gamma m_e c^2/4\sigma_e c U_B \gamma^2 \simeq 5.1 \times 10^8/B^2\gamma$ [sec], where $\sigma_e$, $U_B$, and $\gamma$ denote the Thomson cross-section, magnetic field energy density, and Lorentz factor, respectively. A typical synchrotron frequency can be expressed as $\nu_{\rm sync} = eB\gamma^2/2\pi m_e \simeq 1.2 \times 10^6 B\gamma^2$ [Hz]. Using $t_{\rm cool} \simeq t_{\rm adv}$ in $\gamma_{\rm brk}$, we obtain the following equation by combining these equations,

$$B \simeq 5.9 \times \left(\frac{\nu_{\rm sync}}{1\,{\rm GHz}}\right)^{-1/3} \left(\frac{v_1}{100\,{\rm km/s}}\right)^{2/3} \left(\frac{R}{1\,{\rm kpc}}\right)^{-2/3} [\mu{\rm G}]. \quad (2)$$

Figure 1 shows that there is a spectral turnover at $\nu_{\rm sync} \simeq 1$ GHz. We assumed that the NPS has a spherical structure with an outer diameter $R_{\rm out} \simeq 5$ kpc and an inner diameter $R_{\rm in} \simeq 3$ kpc ($R = R_{\rm out} - R_{\rm in} = 2$ kpc) in the GC model with 8000 pc distance to the NPS, and $R \simeq 2\,{\rm kpc} \times 150/8000 = 38$ pc in the SNR model with 150 pc distance to the NPS. Using the literature value $v_1 \simeq 320$ km/s [3], we obtained $B \simeq 8\,\mu$G in the GC model, whereas unreasonably strong $B \simeq 114\,\mu$G was required in the SNR model.

### 4.2 Spectral Energy Distribution

The Spectral Energy Distribution (SED) analysis was performed for the synchrotron-dominated high galactic-latitude. A region of $(l, b) = (30°, 60°)$ was used, where the spectral region is 1° in both the galactic-longitude and galactic-latitude. Fitting was performed from 22 MHz - 23 GHz, which is pure synchrotron emission, assuming distances to the NPS for each GC (8000 pc) and SNR (150 pc). A leptonic model was used for the fitting [6, 7], assuming the electron distribution as in Equation 1, and using the magnetic field obtained in Section 4.1. The fitting results under these conditions are shown in Figure 2. The dust radiation is represented as $I_\nu = \tau_\nu B_\nu(T)$ with optical thickness $\tau_\nu \sim 10^{-6}$ and temperature $T \sim 20$ K from the literature [8]. The SED of the Fermi Bubbles is shown as reference value fitted with the one-zone leptonic model [3]. The GeV data plots correspond to the emission of the entire bubbles' structure. The radio data plots correspond to the WMAP haze emission averaged over $b = -20°$ to $-30°$, for $|l| < 10°$. The bow-tie centered at 23 GHz K-band indicates the range of synchrotron spectral indices allowed for the WMAP haze. The fitting parameters are listed in Table 1. Inverse Comptonization of the CMB is dominated by high-energy radiation in the GC scenario, with a peak in the 100 - 1000 keV range and a flux of $10^{-9}$ erg s$^{-1}$cm$^{-2}$sr$^{-1}$, whose brightness is almost equal to that of the high-energy band of the Fermi Bubble. However, the IC on the CMB is dominant in the SNR model with a peak below 10 keV and flux of approximately $10^{-12}$ erg s$^{-1}$cm$^{-2}$sr$^{-1}$. This value is several orders of magnitudes lower than the detection limits of modern astronomical satellites [9]. More accurate fitting will be possible if all-sky observations in gamma-rays progress in the future and NPS are discovered.



PoS(Gamma2022)145

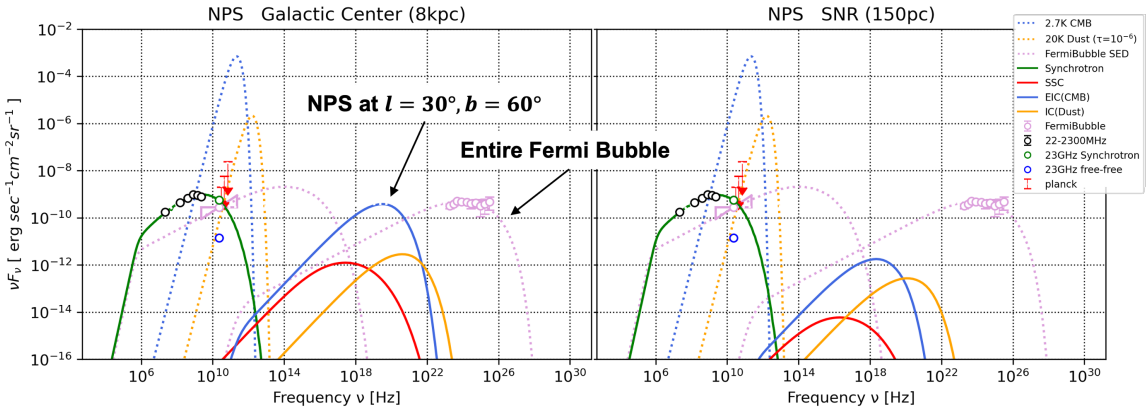


**Figure 2:** SED of the NPS $(l, b) = (30°, 60°)$ in the region of $1° \times 1°$.

**Table 1:** Comparison of fitting parameters of the SED

| Parameter | NPS / GC | NPS / SNR | Fermi Bubbles |
|---|---|---|---|
| Distance [pc] | 8000 | 150 | 8000 |
| $B$ [$\mu$G] | 8 | 114 | 10 |
| Analysis area Radius [cm] | $2.2 \times 10^{20}$ | $4.0 \times 10^{18}$ | $1.2 \times 10^{22}$ |
| $Q_0$ [elec cm$^{-3}\gamma^{-1}$sr$^{-1}$] | $4.0 \times 10^{-4}$ | $5.2 \times 10^{-4}$ | $1.7 \times 10^{-4}$ |
| $\gamma_{\rm min}$ | 1.0 | 1.0 | 1.0 |
| $\gamma_{\rm brk}$ | $1.0 \times 10^{4}$ | $2.7 \times 10^{3}$ | $1.0 \times 10^{6}$ |
| $\gamma_{\rm max}$ | $2.0 \times 10^{4}$ | $5.5 \times 10^{3}$ | $1.0 \times 10^{7}$ |
| Index $s$ | -1.9 | -1.9 | -2.2 |
| $U_e$ [erg cm$^{-3}$] | $1.1 \times 10^{-12}$ | $1.2 \times 10^{-12}$ | $1.8 \times 10^{-13}$ |
| $U_B$ [erg cm$^{-3}$] | $2.5 \times 10^{-12}$ | $5.2 \times 10^{-10}$ | $4.0 \times 10^{-12}$ |
| $P_{\rm n/th}$ [erg cm$^{-3}$] | $1.2 \times 10^{-12}$ | $1.7 \times 10^{-10}$ | $1.4 \times 10^{-12}$ |

### 4.3 NPS non-thermal Energy

In Table 1, $U_e$ and $U_B$ obtained by the fitting are the electron and magnetic field energy densities, and $P_{\rm n/th}$ is the non-thermal pressure, $P_{\rm n/th} = (U_e + U_B)/3$. The non-thermal energy can be estimated by assuming the NPS volume. In the GC model, the total volume of the NPS can be calculated as $V = 4\pi/3 \times (R^3_{\rm out} - R^3_{\rm in}) \sim 1.2 \times 10^{67}$ cm$^3$ using $R_{\rm out} \simeq 5$ kpc and $R_{\rm in} \simeq 3$ kpc. Thus, we estimated that the non-thermal energy of the NPS was $E_{\rm n/th} = V \times (U_e + U_B) \simeq 4.3 \times 10^{55}$ erg. The thermal pressure of the NPS was estimated by [3] using Suzaku observations. It should be noted that they are estimated using $8° < l < 16°$, $42° < b < 48°$ observation data, and obtained $P_{\rm th} \simeq 2 \times 10^{-12}$ erg cm$^{-3}$. It was found to be in close agreement with the non-thermal energy determined for the first time from the radio spectrum of the NPS. Therefore, this can be interpreted naturally in the case of the GC scenario. In constant, in the SNR model, the volume of the NPS was $V \sim 7.9 \times 10^{61}$ cm$^3$, and the non-thermal energy was estimated to be $E_{\rm n/th} \sim 4.1 \times 10^{52}$ erg. Thermal pressure was estimated to be $P_{\rm th} \simeq 1.4 \times 10^{-11}$ erg cm$^{-3}$ which was approximately ten times larger than the non-thermal pressure. Therefore, the pressure balance was found to be disturbed in the



PoS(Gamma2022)145

SNR model. In addition, the typical energy of a supernova remnant is $E \sim 10^{51}$ erg, which is too large, at least for a single SNR. Therefore, if the NPS is a local structure, it could be a massive structure associated with a super bubble [10].

## 5. Conclusion

We analyzed broadband radio observations covering a range between 22 MHz and 70 GHz to provide a systematic analysis of the thermal/non-thermal emissions associated with the NPS. Radio emission of the NPS is composed of synchrotron, free-free, and dust emission. Up to a few GHz, NPS emissions were found to follow a power-law distribution ($T_b \propto \nu^{-\beta}$), with $\beta \simeq 2.6 - 3.0$. In addition, the cut-offs in the radio spectra were found to be approximately 1 GHz, which may indicate that the electron cooling time and advection time are balanced if the spectral turnover is derived from synchrotron cooling. Moreover, the magnetic field of the NPS was estimated as $B \simeq 8\mu$G and $B \simeq 114\mu$G in the GC and SNR models, respectively. In the SED analysis of the high galactic latitude region of the NPS in the GC model, we estimated that gamma-ray emission associated with the NPS, through IC of the CMB, peaked at approximately 100-1000 keV with a flux of $\sim 10^{-9}$ erg cm$^{-2}$s$^{-1}$sr$^{-1}$. However, in the SNR model, IC on the CMB dominates, but with a peak below 10 keV and flux of approximately $\sim 10^{-12}$ erg cm$^{-2}$s$^{-1}$sr$^{-1}$. Using the fitting results, the non-thermal energy of the NPS was calculated to be $E_{\rm n/th} \simeq 4.3 \times 10^{55}$ erg in the GC model. Moreover, it was found that the thermal energy confirmed by [3] in the X-ray band was almost balanced by the newly obtained non-thermal energy in the radio bands. We obtained $E_{\rm n/th} \simeq 4.1 \times 10^{52}$ erg in the SNR model, which indicates that if the NPS radiation originates from a local bubble, it could be super bubble [10]. Future deep surveys in the MeV range may clarify the origin of NPS.

## References

[1] Berkhuijsen, E. M., Haslam, C. G. T., & Salter, C. J. 1971, A&A, 14, 252

[2] Sofue, Y. 1977, A&A, 60, 327

[3] Kataoka, J., Tahara, M., Totani, T., et al. 2013, ApJ, 779, 57. doi:10.1088/0004-637X/779/1/57

[4] Akita, M., Kataoka, J., Arimoto, M., et al. 2018, ApJ, 862, 88. doi:10.3847/1538-4357/aacd08

[5] Gold, B., Odegard, N., Weiland, J. L., et al. 2011, ApJS, 192, 15. doi:10.1088/0067-0049/192/2/15

[6] Inoue, S. & Takahara, F. 1996, ApJ, 463, 555. doi:10.1086/177270

[7] Kataoka, J., Mattox, J. R., Quinn, J., et al. 1999, ApJ, 514, 138. doi:10.1086/306918

[8] Planck Collaboration, Abergel, A., Ade, P. A. R., et al. 2014, A&A, 571, A11. doi:10.1051/0004-6361/201323195

[9] Mitsuda, K., Bautz, M., Inoue, H., et al. 2007, PASJ, 59, S1. doi:10.1093/pasj/59.sp1.S1

[10] Krause, M. G. H., Burkert, A., Diehl, R., et al. 2018, A&A, 619, A120. doi:10.1051/0004-6361/201732416



PoS(Gamma2022)145